Original Article

RPN1: a pan-cancer biomarker and disulfidptosis regulator

Xing Wang[1,2], Hong-Quan Zhu[2], Shi-Ming Lin[2], Bao-Ying Xia[2], Bo Xu[1,3]

[1]Department of General Surgery, The First Affiliated Hospital, Jinan University, Guangzhou, China; [2]Department of General Surgery, Jiangmen Central Hospital, Jiangmen, China; [3]Department of Thyroid Surgery, Guangzhou First People's Hospital, School of Medicine, South China University of Technology, Guangzhou, China

Contributions: (I) Conception and design: X Wang, B Xu; (II) Administrative support: B Xu; (III) Provision of study materials or patients: X Wang, HQ Zhu; (IV) Collection and assembly of data: SM Lin, BY Xia; (V) Data analysis and interpretation: X Wang, HQ Zhu; (VI) Manuscript writing: All authors; (VII) Final approval of manuscript: All authors.

Correspondence to: Bo Xu, MD. Department of General Surgery, The First Affiliated Hospital, Jinan University, No. 613 Huangpu Avenue West, Tianhe District, Guangzhou 510630, China; Department of Thyroid Surgery, Guangzhou First People's Hospital, School of Medicine, South China University of Technology, No. 1 Panfu Road, Yuexiu District, Guangzhou 510180, China. Email: aabb97@163.com.

Background: Elevated expression of SLC7A11, in conjunction with glucose deprivation, has revealed disulfidptosis as an emerging cell death modality. However, the prevalence of disulfidptosis across tumor cell lines, irrespective of SLC7A11 levels, remains uncertain. Additionally, deletion of the ribophorin I (*RPN1*) gene imparts resistance to disulfidptosis, yet the precise mechanism linking *RPN1* to disulfidptosis remains elusive. The aim of this study is to determine the mechanism of *RPN1*-induced disulfidptosis and to determine the possibility of *RPN1* as a pan-cancer marker.

Methods: We hypothesized the widespread occurrence of disulfidptosis in various tumor cells, and proposed that *RPN1*-mediated disulfidptosis may be executed through cell skeleton breakdown. Experimental validation was conducted via flow cytometry, immunofluorescence, and western blot techniques. Furthermore, given *RPN1*'s status as an emerging cell death marker, we utilized bioinformatics to analyze its expression in tumor tissues, clinical relevance, mechanisms within the tumor microenvironment, and potential for immunotherapy.

Results: Conducting experiments on breast cancer (MDA-MB-231) and lung cancer (A549) cell lines under glucose-starved conditions, we found that *RPN1* primarily induces cell skeleton breakdown to facilitate disulfidptosis. *RPN1* demonstrated robust messenger RNA (mRNA) expression across 16 solid tumors, validated by data from 12 tumor types in the Gene Expression Omnibus (GEO). Across 12 cancer types, *RPN1* exhibited significant diagnostic potential, particularly excelling in accuracy for glioblastoma (GBM). Elevated *RPN1* expression in tumor tissues was found to correlate with improved overall survival (OS) in certain cancers [diffuse large B-cell lymphoma (DLBC) and thymoma (THYM)] but poorer prognosis in others [adrenocortical carcinoma (ACC), kidney chromophobe (KICH), brain lower grade glioma (LGG), liver hepatocellular carcinoma (LIHC), and pancreatic adenocarcinoma (PAAD)]. *RPN1* is enriched in immune-related pathways and correlates with immune scores in tumor tissues. In urothelial carcinoma (UCC), *RPN1* demonstrates potential in predicting the efficacy of anti-programmed cell death ligand 1 (PD-L1) immune therapy.

Conclusions: This study underscores *RPN1*'s role in facilitating disulfidptosis, its broad relevance as a pan-cancer biomarker, and its association with the efficacy of anti-PD-L1 immune therapy.

Keywords: Disulfidptosis; ribophorin I (*RPN1*); *SLC7A11*; anti-programmed cell death ligand 1 (anti-PD-L1); pan-cancer

Submitted Apr 08, 2024. Accepted for publication May 15, 2024. Published online May 29, 2024.
doi: 10.21037/tcr-24-581
View this article at: https://dx.doi.org/10.21037/tcr-24-581

Introduction

In the tumor microenvironment, cells face challenges like oxidative stress, metabolic dysregulation, and rapid proliferation (1). Glutathione, crucial for protection, is intricately regulated by cysteine (1). *SLC7A11* facilitates cysteine supply to tumor cells. Blocking cysteine uptake induces ferroptosis, linked to oxidative stress (1). Recent studies revealed cell death from reductive stress (2). Excess cysteine, boosted by *SLC7A11* and glucose deprivation, led to disulfidptosis discovery, marked by abnormal disulfide bond formation in actin, causing F-actin contraction and cell membrane detachment (3). Key genes like *SLC7A11*, *SLC3A2*, ribophorin I (*RPN1*), and *NCKAP1* were identified via CRISPR/Cas9 screening (3). Interestingly, even under glucose-deficient conditions, supplementing excess cysteine in the culture medium of renal cell carcinoma (RCC) cells (786-O) with low *SLC7A11* expression induced disulfidptosis (3). It's unclear if disulfidptosis is widespread in other tumor cell lines. Deleting *RPN1* rendered urothelial carcinoma cells (UMRC6) resistant to disulfidptosis (3), but *RPN1*'s precise role remains unclear.

Cellular oxidative stress triggers typical immune responses (4), paralleled by reactions akin to reductive stress, such as NLRP1 and CARD8-mediated cell pyroptosis (5). Glucose deficiency and reduced ATP levels activate NLRP1 inflammasomes (6), disrupting cytoskeletal function and leading to disulfidptosis (3). Inflammasomes, pivotal in innate immunity, inflammation, and cell death, imply a link between disulfidptosis and immune activation, critical in cancer (7). *RPN1*'s significant role in Arabidopsis innate immunity underscores the interest in exploring its mechanisms and immune implications in disulfidptosis within the tumor microenvironment.

Several studies have investigated the relationship between *RPN1* and cancer. For example, it may promote the progression of breast cancer (8) and be associated with poor prognosis in hepatocellular carcinoma (HCC) (9). However, the biomarker value of *RPN1* across pan-cancers has yet to be investigated.

In this study, we propose that glucose deficiency can induce *RPN1*-dependent disulfidptosis. We observed *RPN1*-dependent disulfidptosis in breast cancer (MDA-MB-231) and lung cancer (A549) cell lines without additional cysteine supplementation. We hypothesize that *RPN1* expression could predict patient outcomes, immune microenvironment, and response to immunotherapy. Through bioinformatics analysis across 33 tumor types, we explore *RPN1*'s clinical relevance, mechanisms in tumor biology, and implications for immunotherapy. *RPN1* gene knockout inhibits disulfidptosis in various cell lines, regardless of *SLC7A11* expression, suggesting *RPN1* as a potential universal cancer therapy target. We present this article in accordance with the MDAR reporting checklist (available at https://tcr.amegroups.com/article/view/10.21037/tcr-24-581/rc).

Highlight box

Key findings

- This research illuminates the pivotal role of ribophorin I (*RPN1*) in promoting disulfidptosis by triggering cell skeleton breakdown. It underscores its broad significance as a biomarker across diverse cancer types and its correlation with the efficacy of immune therapy targeting PD-L1, particularly in urothelial carcinoma.

What is known and what is new?

- Through genome-wide CRISPR/Cas9 screening, key genes contributing to disulfidptosis were identified, including *RPN1*. However, the precise mechanism by which *RPN1* influences disulfidptosis remains unclear. It is known that *RPN1* plays a crucial role in innate immunity in Arabidopsis, yet whether *RPN1* serves as a novel cancer biomarker and its association with the efficacy of immunotherapy remain elusive.

What is the implication, and what should change now?

- The findings of this study underscore the mechanism by which *RPN1* promotes disulfidptosis through inducing cell skeleton protein breakdown, emphasizing its impact on diagnosis, prognosis, and immune checkpoint inhibitor therapy in the context of pan-cancer scenarios. We demonstrate the inhibition of disulfidptosis upon *RPN1* gene knockout in cell lines not previously validated, irrespective of *SLC7A11* expression levels, providing additional evidence for *RPN1* as a potential universal target for cancer therapy. Future research should explore whether other metabolic stress conditions can lower intracellular NADPH levels, thus inducing disulfidptosis. Additionally, our study highlights the potential of *RPN1* as an immune therapy marker, necessitating further validation of its role in cohorts.

Methods

Figure 1 depicts the workflow employed in this study. The study was conducted in accordance with the Declaration of Helsinki (as revised in 2013).

Cell lines and culture

All cell lines used in this study were originally obtained from the American Type Culture Collection (ATCC; Manassas, VA, USA) as follows: HEK-293T, A549, and

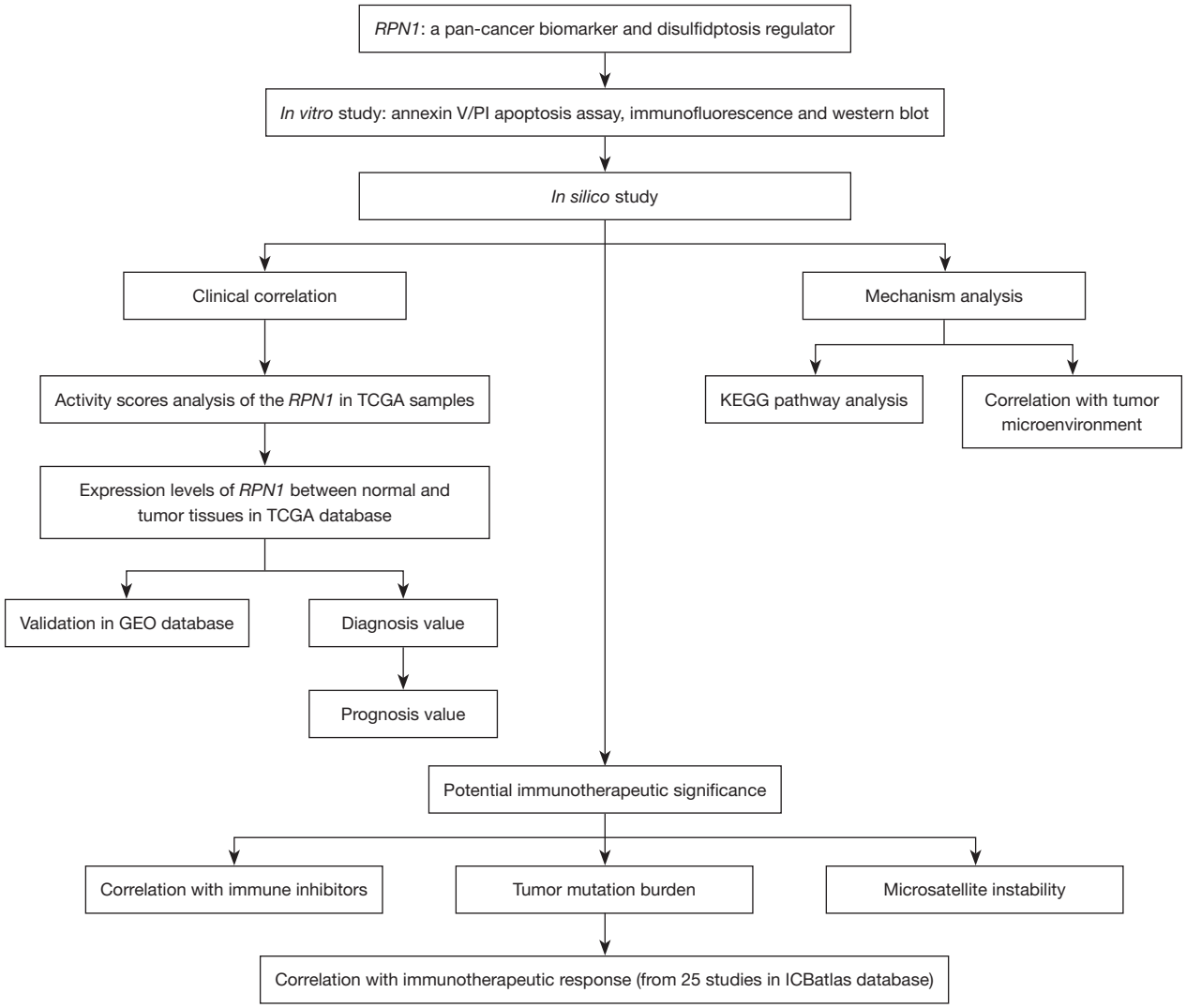

Figure 1 Workflow of the study. *RPN1*, ribophorin I; PI, propidium iodide; TCGA, The Cancer Genome Atlas; GEO, Gene Expression Omnibus; KEGG, Kyoto Encyclopedia of Genes and Genomes.

MDA-MB-231. All cells were incubated in humidified air at 37 ℃ with 5% CO_2. The cell lines were cultured in Dulbecco's modified Eagle medium (DMEM; Gibco, Waltham, MA, USA) with 10% fetal bovine serum (FBS), 100 U/mL of penicillin and 100 μg/mL of streptomycin. All cell lines used in this study were regularly authenticated by the short tandem repeat (STR) method and had not been in culture for more than 2 months.

Gene knockout in cell lines

Plasmid

The single guide RNA (sgRNA) expression constructs were cloned into the LentiCrispr-V2-puro backbone. The sequences of the sgRNAs used in this study were as follows: *RPN1*-sg1 (5'-TGTAGGCAACAATCACAGGG-3'), *RPN1*-sg2 (5'-TGAGGACGTGAAGCGCACAG-3').

Lentivirus package

The 293T cell line was seeded into a 6-well plate and cultured until a confluency of 70% was achieved. For the transfection procedure, tube A contained a mixture of the target gene plasmid, psPAX2, and pMD2.G, suspended in 150 μL of Opti-MEM medium at a ratio of 3 μg:2 μg:1 μg. Concurrently, tube B was prepared with 24 μL of polyethylenimine (PEI) added to an equal volume of Opti-

MEM medium. After a 30-minute incubation period to allow for complex formation, the mixture was added to the cells. The culture medium was replaced with complete medium (with 10% FBS, 100 U/mL of penicillin and 100 µg/mL of streptomycin). At 48 hours post-transfection, the supernatant was collected and cleared of cellular debris using a 0.45-µm filter membrane. The lentivirus present in the supernatant was then concentrated using the Lenti-Pac Lentivirus Concentration Solution (GeneCopoeia, LT007, Rockville, MD, USA), in preparation for subsequent gene knockout experiments.

Lentiviral infection

Cell lines designated for infection were plated in 6-well plates and allowed to reach 70% confluency prior to the initiation of the lentiviral infection assay. Prepared lentiviral solution was then added to the culture dishes. After 24 hours, the medium was replaced, and at 72 hours post-infection, selection with puromycin commenced. Following 2 weeks of selection, stable transfectants were successfully established.

Apoptosis assay

A549 and MDA-MB-231 cells stably knocking down *RPN1* were collected and rinsed twice with phosphate-buffered saline (PBS), and stained with propidium iodide (PI; KGA-108; KeyGen, Changchun, China) for 30 minutes at room temperature. Stained cells were then examined by flow cytometry and results were analyzed with FlowJo software [Becton, Dickinson and Co. (BD), Franklin Lakes, NJ, USA]. The apoptosis assay was repeated a total of three times, including both technical and biological replicates.

Immunofluorescence

Cells were seeded into glass-bottomed culture dishes (801002; NEST Biotechnology, Wuxi, China) 1 day before experiments. Cells were fixed with 4% paraformaldehyde for 15 minutes without permeabilization and blocked with 3% bovine serum albumin for 30 minutes at room temperature, and rinsed twice with PBS between the interval step. Next, the cells were incubated with the phalloidin (PHDH1; Cytoskeleton, Denver, CO, USA) for 2 hours at room temperature or overnight at 4 ℃. After rinsing three times with PBS, the cells were incubated for 2 hours at room temperature with the following secondary antibodies: anti-mouse Alexa Fluor-594. Nuclei were stained with Hoechst 33342 for 5 minutes (Molecular Probes, Invitrogen, Carlsbad, CA, USA). The cells were imaged using laser scanning confocal microscopes (LSM880, ZEN2.6, 63× oil lens; ZEISS, Oberkochen, Germany).

Western blotting

Cells were harvested and lysed in radioimmunoprecipitation assay (RIPA) buffer [50 mM Tris-HCl pH 7.5, 150 mM NaCl, 1 mM ethylenediaminetetraacetic acid (EDTA), 1% NP40] containing Protease Inhibitors Cocktails set I and Phosphatase Inhibitor Cocktails set II (Sigma-Aldrich, Darmstadt, Germany), and centrifuged at 12,000 rpm/min for 20 minutes at 4 ℃. The cell lysates were then boiled in gel loading buffer for 10 minutes and resolved by 10% sodium dodecyl sulfate polyacrylamide gel electrophoresis (SDS-PAGE). The proteins were transferred to polyvinylidene fluoride (PVDF) membranes (Millipore, Burlington, MA, USA), which were then blocked in PBS with 5% non-fat milk and 0.1% Tween-20 and immunoblotted with primary antibodies overnight at 4 ℃. Horseradish peroxidase-conjugated secondary antibodies were used, and high-signal enhanced chemiluminescence (ECL) substrate (Tanon, Shanghai, China) was used for detection. Primary antibodies were used: *RPN1* (12894-1-AP, 1:1,000; Proteintech, Rosemont, IL, USA), *FLNA* [4762S, 1:1,000; Cell Signaling Technology (CST), Danvers, MA, USA], *FLNB* (12979S, 1:2,000; CST), myosin IIa (*MYH9*; 3403S, 1:1,000; CST), *TLN1* (4021S, 1:1,000; CST), Drebrin (10260-1-AP, 1:2,000; Proteintech), and actin (MA5-11869, 1:500; Thermo Fisher, Waltham, MA, USA).

Data collection

To comprehensively analyze tumor samples, we obtained genomic, somatic mutation-related, and clinicopathological information from multiple databases. The Cancer Genome Atlas (TCGA) database (10), accessed through the University of California Santa Cruz Xena browser (http://xena.ucsc.edu/), provided a large dataset of 15,776 samples from 33 cancer types (the tumor types and their abbreviations are listed in Table S1) and normal tissues, enabling robust statistical analyses and meaningful conclusions about various types of cancer. To validate our results, we searched for 12 additional datasets from the Gene Expression Omnibus (GEO) database (https://www.ncbi.nlm.nih.gov/geo/) (11), providing diverse samples and confirming reproducibility across different cohorts. The process of selecting datasets begins with identifying cancer

types that match those in TCGA, such as "squamous cell carcinoma of the lung", rather than broadly categorizing them as "lung cancer". Next, we choose the largest available dataset for this specific cancer type. The reason we only validated in 12 microarray datasets is because validation was not successful in the other four types of cancer, possibly due to insufficient available datasets for these four types of cancer. Table S2 includes detailed information on the GEO datasets used in this study. The integration of multiple databases and datasets ensures a comprehensive analysis of tumor samples and strengthens the validity of our findings.

Comparing the expression and activity levels of RPN1 between normal and tumor tissues across the TCGA and GEO databases

To investigate the biological function of a gene, it is essential to have a certain level of baseline expression. Therefore, we first calculated the median expression level of *RPN1* in each cancer type using the "limma" package in R and compared its expression difference between normal and cancer tissues. The gene expression levels were normalized using the fragments per kilobase per million (FPKM) algorithm.

To ensure adequate gene activity for proper biological function, we assessed *RPN1* activity in pan-cancer using the "GSVA" package (12). The package identified 100 genes co-expressed with *RPN1* using the Pearson correlation test. Then, these gene sets were matched to a predefined gene set using single-sample gene set enrichment analysis (GSEA), and their expression statistics were aggregated into activity scores using the Gaussian algorithm. Similarly, *RPN1* activity was also compared between tumor and normal tissues.

Clinical correlation of RPN1

We conducted a stratified analysis using age, gender, and disease stage to investigate the correlation between *RPN1* mRNA expression and clinical parameters. Receiver operating characteristic (ROC) curves and areas under the curve (AUCs) were used to evaluate the diagnostic value of *RPN1* in pan-cancer, utilizing the "pROC" package in R software, through the online tool Xiantao Academic (https://www.xiantao.love/). The overall survival (OS) of the TCGA pan-cancer cohort were assessed using univariate Cox regression with hazard ratios (HRs) and Kaplan-Meier (KM) method with log-rank test, using the "survival" package.

Kyoto Encyclopedia of Genes and Genomes (KEGG) pathway analysis

To explore the signaling pathways related to *RPN1*, we retrieved the different pathways between low and high expression groups for the *RPN1* gene in pan-cancer from the KEGG database and performed GSEA. To determine statistical significance, we used corrected false discovery rates (FDRs) of <0.05 and absolute $\log_2$ fold changes of ≥1. The c2.cp.kegg.v7.4.symbols were utilized for pathway analysis as the annotation reference sets. The top 5 signaling pathways with the highest normalized enrichment scores (NESs) were visualized using the "enrichplot" package. This particular part of the enrichment analysis was executed utilizing the "org.Hs.eg.db" package.

Correlation between RPN1 and tumor microenvironment

The Estimation of Stromal and Immune cells in Malignant Tumors using Expression data (ESTIMATE) package (13), a specialized tool for evaluating the extent of stromal and immune cell infiltration in the tumor microenvironment, was employed to analyze the tumor microenvironment and its association with *RPN1* expression levels. Utilizing this package, stromal and immune scores were computed for each individual sample, serving as indicators of cell infiltration within the tumor microenvironment. Higher scores indicated greater levels of cell infiltration in the corresponding samples. To assess the relationship between *RPN1* expression levels and the stromal or immune scores, correlation coefficients and P values were employed as metrics.

Furthermore, the Cell-type Identification by Estimating Relative Subsets of RNA Transcripts (CIBERSORT) package (14) was utilized to estimate the composition of the 22 distinct immune cell types infiltrating the tumor. This estimation was based on a deconvolution algorithm enabling the quantification of immune cell proportions within the tumor microenvironment. The correlation between the presence of these immune cell types and *RPN1* expression levels was examined. A correlation coefficient threshold of ≥0.3 and a P value threshold of <0.001 were applied to ascertain the statistical significance of the correlations during this two-stage analysis.

Potential immunotherapeutic implication of RPN1

The association between immune treatment response and various indicators, such as immune inhibitors, tumor mutation

burden (TMB), and microsatellite instability (MSI), has been well established. In our study, we aimed to investigate the correlations between the expression levels of *RPN1* and these indicators, with the objective of better understanding their potential role in immune response. To explore the relationship between *RPN1* and immune inhibitors, we utilized the Tumor-Immune System Interaction Database (TISIDB) online database (http://cis.hku.hk/TISIDB/index.php). TMB, defined as the total number of somatic gene coding errors, base substitutions, insertions, or deletions detected per million bases, was quantified for each case by dividing the total number of mutations by the exome size (38 Mb). MSI scores were obtained from previously published studies for TCGA cancer cases (15). To visualize the results, we employed the "fmsb" package. Additionally, we evaluated the differential expression of *RPN1* between the responder and non-responder groups, encompassing a total of 25 clinical studies on immune therapy. These studies specifically investigated the effectiveness of anti-programmed cell death 1 (PD-1), anti-programmed cell death ligand 1 (PD-L1), and anti-CTLA4 immunotherapy. Our objective was to assess whether *RPN1* could serve as a predictive marker for immunotherapy efficacy. Detailed information about these clinical studies can be found in Table S3. To perform this analysis, we utilized the online database ICBatlas (http://bioinfo.life.hust.edu.cn/ICBatlas/) and visualized the results using the online tool Xiantao Academic (https://www.xiantao.love/).

Statistical analysis

All statistical analyses in this study were performed using R software (version 4.2.2; r Foundation for Statistical Computing, Vienna, Austria). Either the Student's *t*-test or the Wilcoxon rank-sum test was employed to assess continuous variables, depending on data distribution. In cases where the data did not follow a Gaussian distribution, the Mann-Whitney test was utilized. Categorical clinicopathological characteristics were compared using the Chi-square test or Fisher's exact test. Pearson correlation analysis was conducted for correlation analysis. Statistical significance was determined by P values of <0.05 or <0.01.

Results

RPN1 induced cell death under glucose-free condition in disulfidptosis

In *Figure 2*, the experimental results indicate that under glucose deprivation conditions, *RPN1* induces disulfidptosis. Initially, we employed flow cytometry to analyze cell death in wild-type (WT) and *RPN1*-knockout (KO)1/KO2 MDA-MB-231 as well as A549 cells (Figure S1) cultured in glucose-containing (+Glc) or glucose-deficient (–Glc) media (*Figure 2A*). This analysis revealed the impact of glucose availability on cell survival. In glucose deficiency, cell death increased, a phenomenon mitigated by *RPN1* knockout. Hence, the conclusion is drawn that *RPN1* serves as a promoter of cell death. To further elucidate cellular changes, we utilized immunofluorescence labeling of F-actin with fluorescent phalloidin in +Glc or –Glc media to examine WT and *RPN1*-KO MDA-MB-231 as well as A549 cells (*Figure 2B*). This enabled visualization of alterations in the actin cytoskeleton under different glucose conditions. In glucose deprivation, cell death and cytoskeletal breakdown were observed. Upon *RPN1* knockout, this cytoskeletal breakdown was suppressed, indicating that *RPN1* mediates cell death through the degradation of cytoskeletal proteins. Protein extraction and western blot analysis using non-reducing and reducing methods were conducted to study the expression of indicative cytoskeletal proteins in normal control (NC) and *RPN1*-KO MDA-MB-231 as well as A549 cells cultured in +Glc or –Glc media (*Figure 2C*). Under glucose deprivation, the absence of *RPN1* contributed to increased stability of cytoskeletal proteins (FLNA, FLNB, MYH9, TLN1, Drebrin, and Actin, *Figure 2C*). This demonstrates that *RPN1* loss contributes to the maintenance of cytoskeletal integrity. These findings collectively underscore the role of *RPN1* in mediating disulfidptosis, possibly through mechanisms involving the induction of cytoskeletal protein degradation.

Differential expressions and activity of RPN1 were found in cancerous and normal tissues in 12 cancer types

Figure 3A depicts the expression pattern of *RPN1* in 33 cancer tissues from TCGA databases, demonstrating robust mRNA expression levels (>5 FPKM normalized) in most solid tumors. Moreover, significant differences were observed between tumor and adjacent non-tumor tissues in 16 specific cancer types. Notably, BLCA, BRCA, CESC, CHOL, COAD, ESCA, GBM, HNSC, KIRP, LIHC, LUAD, LUSC, PRAD, READ, STAD, and UCEC exhibited higher expression levels in tumor tissues compared to adjacent non-tumor tissues (*Figure 3B*). In terms of gene activity, *RPN1* exhibited robust activity in all 33 tumor tissues (*Figure 3C*). In comparison to adjacent

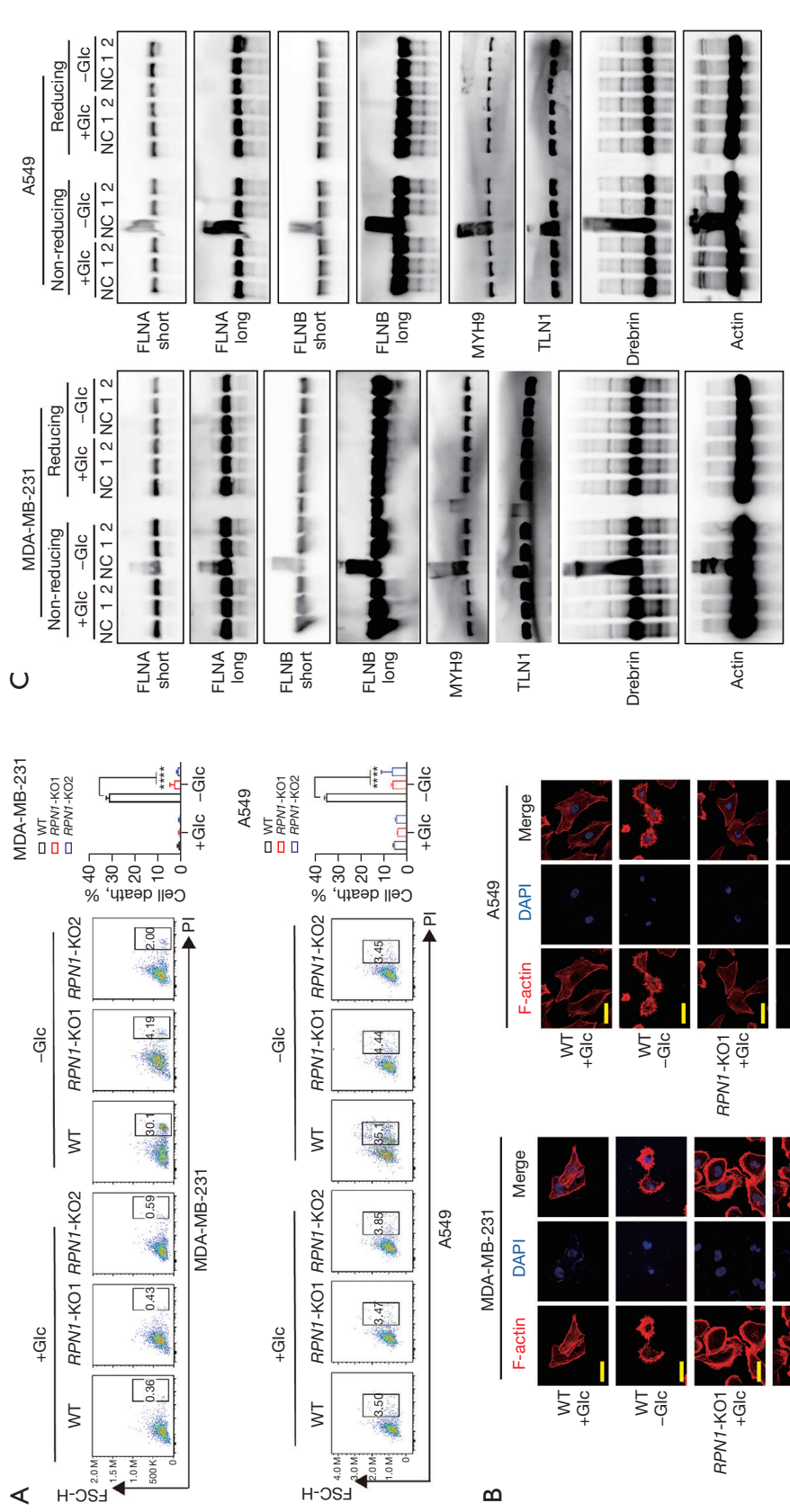

Figure 2 *RPN1*-induced cell death under glucose-free condition in disulfidptosis. (A) Flow cytometry analysis of cell death in WT and *RPN1*-KO1/KO2 MDA-MB-231 and A549 cells cultured in medium +Glc or −Glc. (B) Immunofluorescence of F-actin with phalloidin in WT and *RPN1*-KO cells MDA-MB-231 and A549 cultured in medium +Glc or −Glc glucose. Note: The yellow scale represents 10 μm. (C) Western blot analysis of the indicated actin cytoskeleton proteins in NC and *RPN1*-KO MDA-MB-231 and A549 cells cultured in medium +Glc or −Glc by nonreducing and reducing methods. ****, P<0.001. FSC-H, forward scatter-height; PI, propidium iodide; WT, wild type; KO, knockout; *RPN1*, ribophorin I; +Glc, with glucose; −Glc, without glucose; NC, negative control.

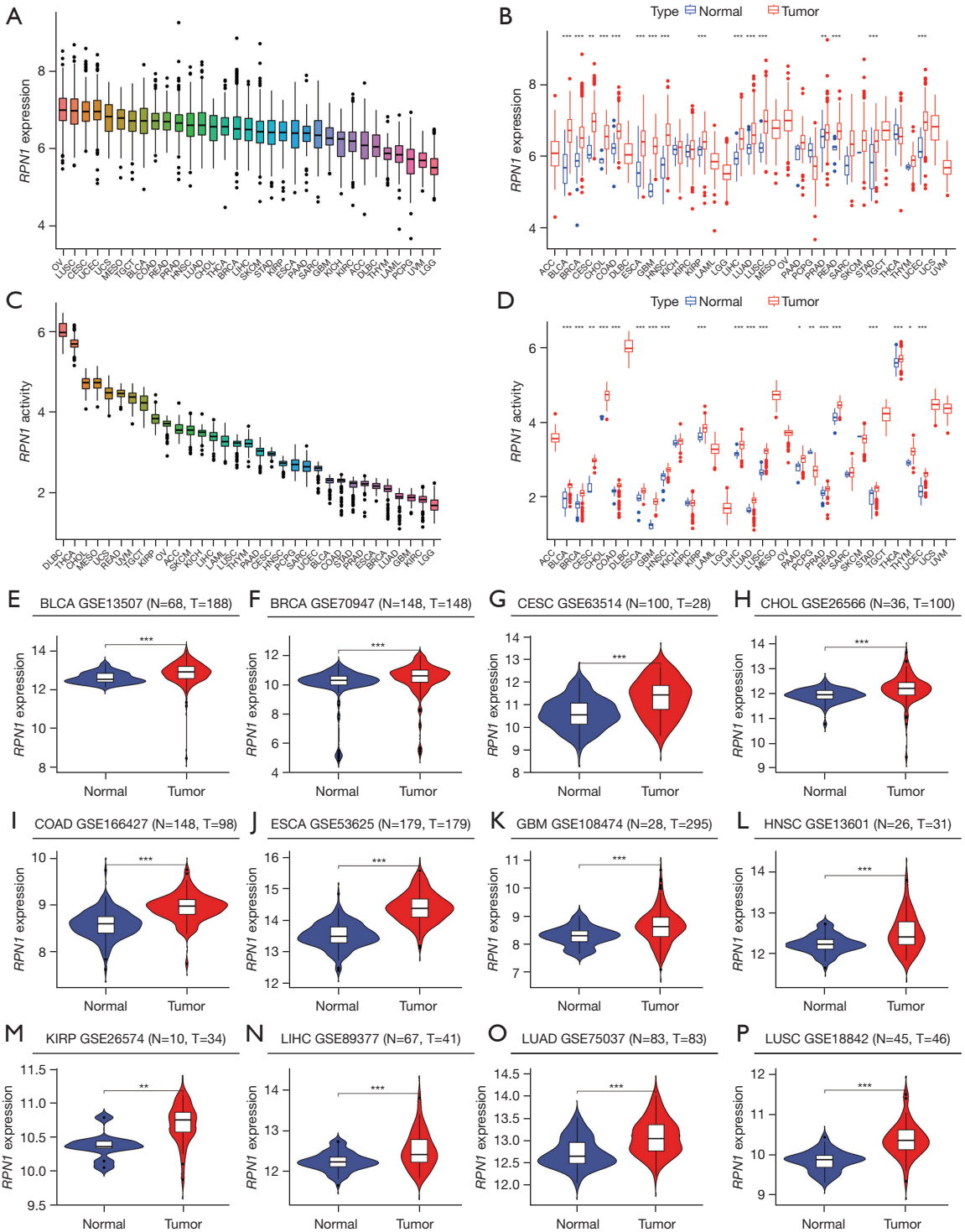

Figure 3 Expression and activity of *RPN1* genes—TCGA data and GEO database validation. (A) Mean *RPN1* expression levels in tumor tissues of pan-cancer in TCGA (FPKM normalized). (B) Differential expression levels of *RPN1* between normal and tumor tissues in TCGA pan-cancer. (C) Activity scores of *RPN1* of individual cancer type from TCGA (Gaussian algorithm using ssGSEA approach). (D) Differential activity levels of *RPN1* between normal and tumor tissues in TCGA pan-cancer. Independent validation of expression levels of *RPN1* between normal and tumor tissues in BLCA (E), BRCA (F), CESC (G), CHOL (H), COAD (I), ESCA (J), GBM (K), HNSC (L), KIRP (M), LIHC (N), LUAD (O), and LUSC (P) databases from GEO. Comparisons between groups were made using the Mann-Whitney test, and data were presented using means ± SEMs. *, P<0.05; **, P<0.01; ***, P<0.001. *RPN1*, ribophorin I; TCGA, The Cancer Genome Atlas; GEO, Gene Expression Omnibus; FPKM, fragments per kilobase per million; ssGSEA, single sample gene set enrichment analysis; SEM, standard error of the mean.

non-tumor tissues, as illustrated in *Figure 3D*, *RPN1* activity was generally higher in 19 tumor types, including BLCA, BRCA, CESC, CHOL, COAD, ESCA, GBM, HNSC, KIRP, LIHC, LUAD, LUSC, PAAD, PRAD, READ, STAD, THCA, THYM, and UCEC. This was corroborated by the differential expression levels of genes in the two tissue types, providing mutual validation of the results.

To validate the differential mRNA expression of *RPN1* observed in the 12 tumor types with significant differences between tumor and adjacent non-tumor tissues, we utilized the GEO database for validation. As illustrated in *Figure 3E-3P*, the mRNA expression trends of *RPN1* in 12 tumor types (including BLCA, BRCA, CESC, CHOL, COAD, ESCA, GBM, HNSC, KIRP, LIHC, LUAD, and LUSC) were consistent with the findings from the TCGA database across multiple validation datasets. Due to limited data availability in GEO, further validation of expression in PRAD, READ, STAD, and UCEC was not feasible.

RPN1 has moderate diagnostic and prognostic value

Using normal tissue samples from the TCGA database as a reference, we assessed the diagnostic potential of *RPN1* (*Figure 4A-4J*). Our analysis revealed significant diagnostic value (AUC >0.8) for *RPN1* in BLCA, BRCA, CESC, CHOL, COAD, ESCA, GBM, HNSC, LIHC, and LUSC. Notably, in the case of GBM (*Figure 4G*), the AUC reached an impressive value of 0.978, potentially influenced by the relatively small sample size in this dataset, comprising only five normal tissues and 174 tumor tissues.

Additionally, the univariate Cox regression model indicated that high *RPN1* expression in tumor tissues was associated with improved OS in DLBC [HR =0.080, 95% confidence interval (CI): 0.010–0.631, P=0.02, *Figure 4K*], and THYM (HR =0.086, 95% CI: 0.010–0.773, P=0.03, *Figure 4K*). However, it was linked to poorer prognosis in ACC (HR =2.683, 95% CI: 1.275–5.646, P=0.009), KICH (HR =7.021, 95% CI: 1.124–43.865, P=0.04), LGG (HR =3.828, 95% CI: 2.173–6.744, P<0.001), LIHC (HR =2.107, 95% CI: 1.392–3.189, P<0.001), and PAAD (HR =1.713, 95% CI: 1.016–2.891, P=0.04). These findings were partially corroborated by KM survival curves (*Figure 4L-4O*). Intriguingly, *RPN1* exhibited favorable attributes in terms of expression profiling, diagnostic value, and prognostic significance across multiple cancer types, emphasizing its potential as a highly promising biomarker in this tumor context.

KEGG pathway and tumor microenvironment analyses show strong correlations between RPN1 expressions and immune response

To investigate potential mechanisms, we performed KEGG pathway enrichment analysis on different expression groups of *RPN1* in eight validated cancer types (*Figure 5*, Table S4). Interestingly, regardless of the expression pattern, *RPN1* was found to be enriched in immune-related pathways across multiple cancers. For example, it showed enrichment in the antigen processing and presentation pathway (NES =1.891, P=0.02, FDR q-value =0.405 in CESC; NES =1.728, P=0.013, FDR q-value =0.38 in LUSC), graft-versus-host disease (NES =1.735, P=0.026, FDR q-value =0.67 in KIRP; NES =1.787, P=0.038, FDR q-value =0.599 in BRCA), and RIG-I-like receptor signaling pathway (NES =1.921, P=0.017, FDR q-value =0.405 in CESC; NES =−1.422, P=0.01, FDR q-value =0.67 in COAD; NES =−1.775, P=0.013, FDR q-value =0.342 in LUAD; and NES =1.703, P=0.013, FDR q-value =0.380 in LUSC).

These findings prompted us to further investigate the relationship between *RPN1* expression and the tumor microenvironment (*Figure 6*). Firstly, the ESTIMATE scoring system demonstrated a positive correlation between *RPN1* expression and immune scores in LGG and SARC tumors (*Figure 6A*,*6F*), while it showed a negative correlation with PAAD (*Figure 6D*). Additionally, the CIBERSORT algorithm revealed correlations between *RPN1* expression and the infiltration levels of various immune cells in multiple tumor tissues (*Figure 6G-6O*), although the distribution of this correlation appeared to be scattered and lacked a clear pattern. In summary, the preliminary mechanistic analysis results indicate a correlation between *RPN1* and immune responses in tumor tissues, suggesting the need for further exploration of potential immune therapeutic responses.

RPN1 expression potentially predicts immunotherapy efficacy for non-small cell lung cancer (NSCLC), RCC, and SKCM

After utilizing the TISIDB database, we identified notable correlations involving *RPN1* expression in specific cancer types. In GBM, *RPN1* expression displayed a positive correlation with the immune checkpoint *IL10RB* expression, whereas it exhibited a negative correlation with *TGFBR1* expression (*Figure 7A*). Moreover, *RPN1* expression showed significant correlations with TMB in THCA, STAD, SKCM,

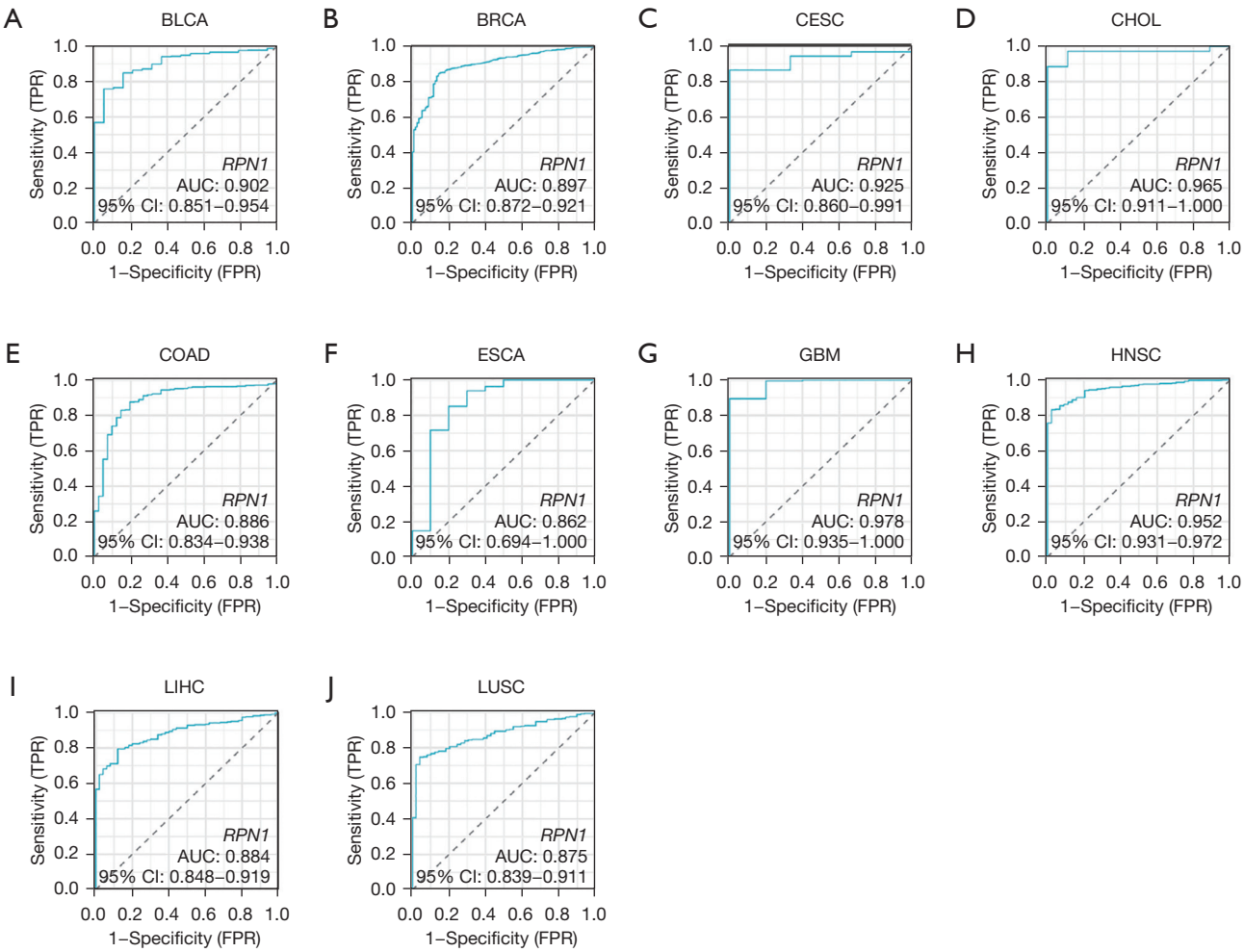

K

Overall survival

	P value	Hazard ratio
ACC	0.009	2.683 (1.275–5.646)
BLCA	0.20	1.235 (0.893–1.706)
BRCA	0.27	0.814 (0.565–1.174)
CESC	0.52	0.839 (0.492–1.431)
CHOL	0.56	1.337 (0.503–3.553)
COAD	0.29	1.354 (0.770–2.381)
DLBC	0.02	0.080 (0.010–0.631)
ESCA	0.29	1.325 (0.787–2.229)
GBM	0.26	1.312 (0.816–2.110)
HNSC	0.23	1.193 (0.894–1.592)
KICH	0.04	7.021 (1.124–43.865)
KIRC	0.29	1.227 (0.842–1.789)
KIRP	0.16	1.827 (0.794–4.202)
LAML	0.84	1.055 (0.636–1.750)
LGG	<0.001	3.828 (2.173–6.744)
LIHC	<0.001	2.107 (1.392–3.189)
LUAD	0.86	0.969 (0.688–1.364)
LUSC	0.73	1.050 (0.793–1.390)
MESO	0.57	1.179 (0.671–2.072)
OV	0.23	0.841 (0.636–1.113)
PAAD	0.04	1.713 (1.016–2.891)
PCPG	0.66	0.710 (0.157–3.214)
PRAD	0.55	1.468 (0.412–5.229)
READ	0.63	0.757 (0.243–2.357)
SARC	0.054	1.423 (0.994–2.039)
SKCM	0.20	0.841 (0.644–1.098)
STAD	0.43	0.878 (0.636–1.211)
TGCT	0.21	6.927 (0.341–140.831)
THCA	0.93	1.067 (0.250–4.550)
THYM	0.03	0.086 (0.010–0.773)
UCEC	0.80	1.062 (0.662–1.705)
UCS	0.56	0.766 (0.312–1.880)
UVM	0.19	0.386 (0.093–1.603)

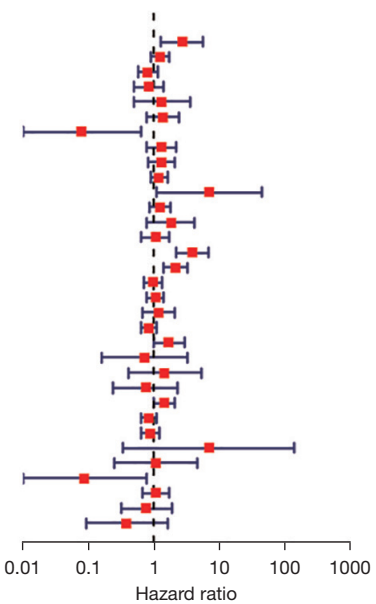

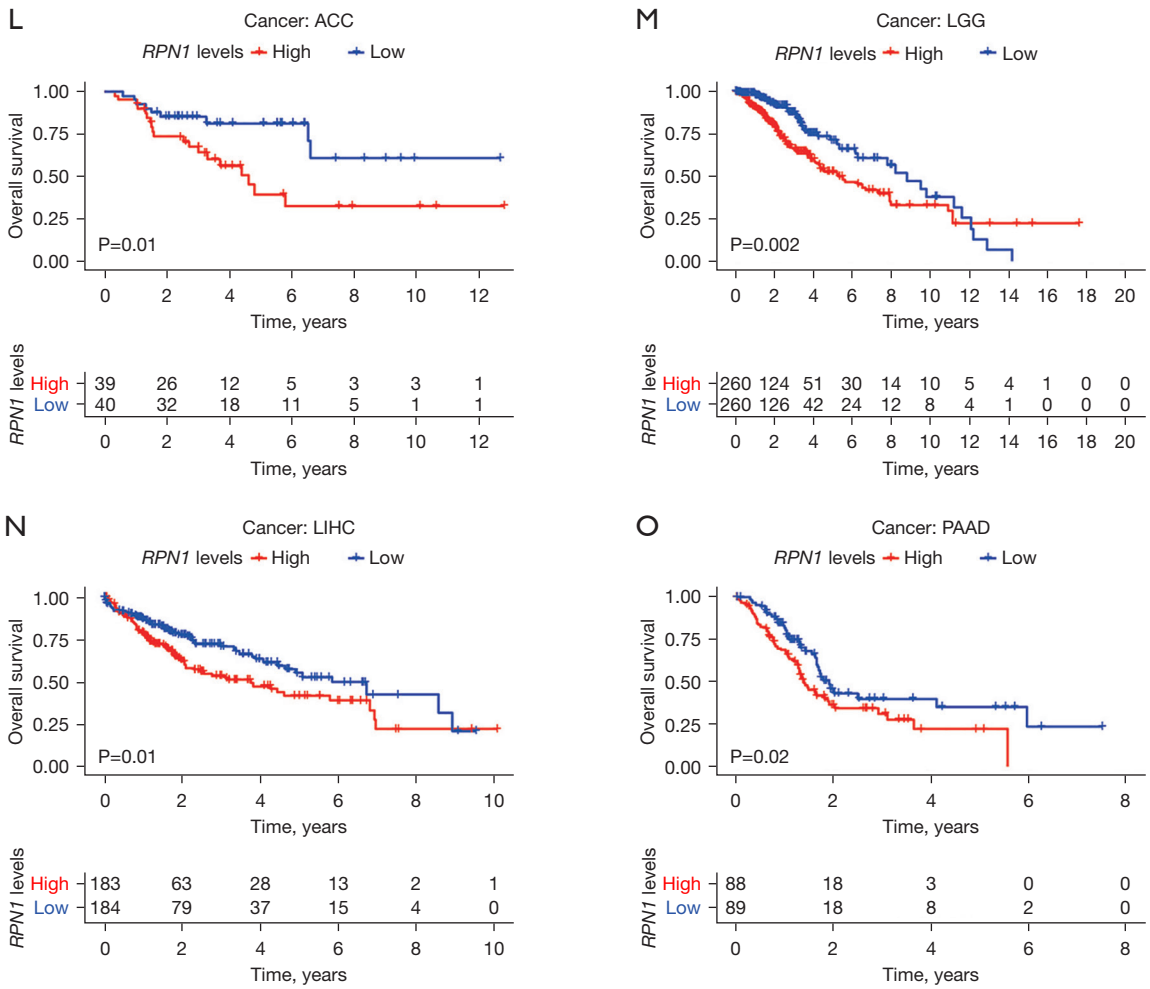

Figure 4 Clinical relationship of *RPN1* and pan-cancer in TCGA database. (A-J) ROC curve for *RPN1* in pan-cancer (using TCGA normal samples as reference). Analysis of prognostic value by using the forest (K) and Kaplan-Meier plots (L-O) of *RPN1* in pan-cancer. Univariate Cox regression with HR was used to investigate the prognostic values of (K) *RPN1* expression levels. P values of <0.05 indicated that the proportional hazards assumption was not violated. The genetic risk is expressed using the HR and 95% CI. Kaplan-Meier curves were used to validate the findings of the forest plot for (L-O) *RPN1* in variable tumor types. The log rank test result was statistically significant with a P value of <0.05. TPR, true positive rate; FPR, false positive rate; *RPN1*, ribophorin I; AUC, area under the curve; CI, confidence interval; TCGA, The Cancer Genome Atlas; ROC, receiver operating characteristic; HR, hazard ratio.

SARC, PAAD, LUSC, LUAD, LIHC, LGG, LAML, HNSC, DLBC, COAD, BRCA, and BLCA (*Figure 7B*). Similarly, *RPN1* expression exhibited correlations with MSI scores in UCS, UCEC, STAD, LUSC, LUAD, LGG, HNSC, and BLCA (*Figure 7C*).

Furthermore, *Figure 7D* demonstrates the differential expressions of *RPN1* in responder and non-responder groups across an anti-PD-L1 cohort. Specifically, responders with urothelial carcinoma (IMvigor210 study) exhibited up-regulated *RPN1* expression.

Discussion

The *RPN1* gene encodes a type I integral membrane protein found exclusively in the rough endoplasmic reticulum (16). It plays a crucial role as part of an N-oligosaccharyl transferase complex, which links high mannose oligosaccharides to asparagine residues within the Asn-X-Ser/Thr consensus motif of nascent polypeptide chains (16). This process is essential for protein N-glycosylation. The UMRC6 cells' increased resistance to disulfidptosis upon *RPN1* knockdown suggests that *RPN1* may be involved in regulating cell

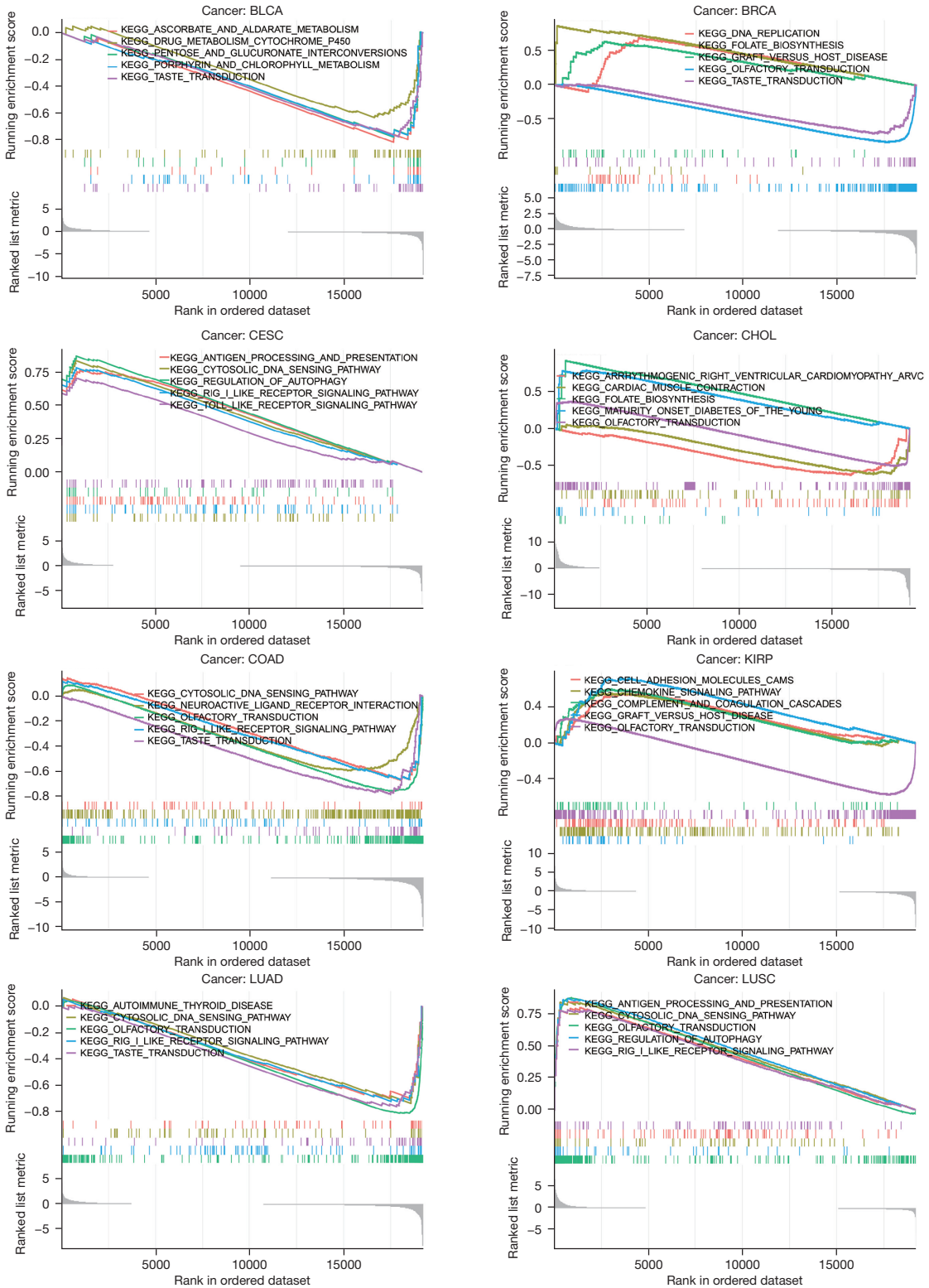

Figure 5 KEGG functional enrichment analyses of *RPN1* in pan-cancer. For each panel, the pathways marked on the left were enriched in the high-target gene expression group, while the pathways marked on the right were enriched in the low-target gene expression group. KEGG, Kyoto Encyclopedia of Genes and Genomes; *RPN1*, ribophorin I.

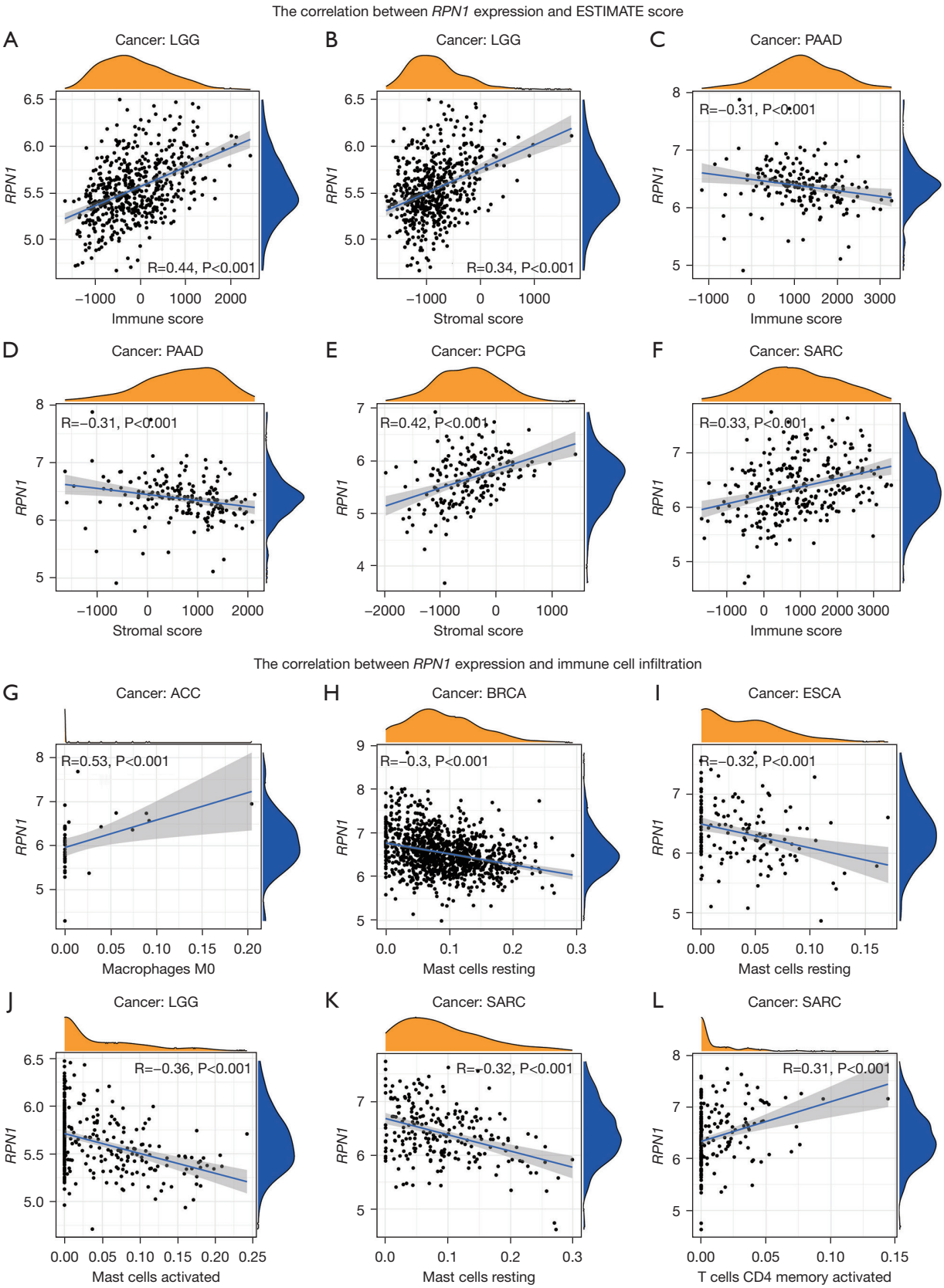

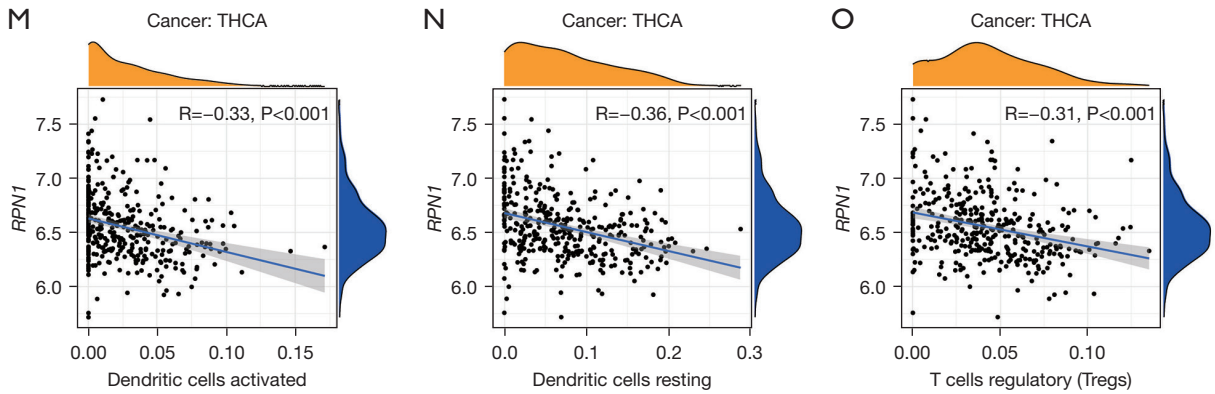

Figure 6 The correlation between *RPN1* expression and ESTIMATE score and relationship of immune cell infiltration. (A-F) The correlation between *RPN1* expression and ESTIMATE score in LGG, PAAD, PCPG, and SARC tissues. The ESTIMATE score includes stromal score (indicating the presence of stromal cells in tumor tissue) and immune score (indicating the infiltration of immune cells in tumor tissue). Assess the correlation between *RPN1* expression levels and stromal or immune scores. The higher the correlation coefficient (R value), the stronger the correlation between *RPN1* expression and stromal cells or immune cell infiltration. (G-O) The correlation between *RPN1* expression and immune cell infiltration in ACC, BRCA, ESCA, LGG, SARC, and THCA tissues. Use the CIBERSORT algorithm to calculate the relationship between *RPN1* expression and the degree of infiltration of various immune cells. Similarly, a higher R value indicates a stronger correlation between this gene and specific types of immune cells in the corresponding tumor tissue. If the absolute value of R is greater than 0.3, a correlation scatter plot will be generated. *RPN1*, ribophorin I; ESTIMATE, Estimation of Stromal and Immune cells in Malignant Tumors using Expression data; CIBERSORT, Cell-type Identification by Estimating Relative Subsets of RNA Transcripts.

survival pathways (3). However, the precise underlying mechanism remains unclear. In this study, we elucidated the previously unreported mechanistic role of *RPN1* in inducing disulfidptosis. Through an investigation into cell death under glucose starvation in breast and lung cancer cell lines, we clarified the role of *RPN1* in this process, primarily by inducing cell skeleton breakdown to promote disulfidptosis. To our knowledge, this study represents the first exploration of *RPN1*'s specific mechanism in disulfidptosis.

The relationship between *RPN1* and cancer has been partially elucidated. For instance, *RPN1* promotes proliferation, migration, and invasion of breast cancer cells through the *PI3K/AKT/mTOR* signaling pathway (8), possibly by inhibiting apoptosis triggered by endoplasmic reticulum stress (17). In HCC, survival analysis shows that high *RPN1* expression is associated with adverse OS in HCC patients (9). Zheng *et al.* found that the Circ-SNX27 sponging miR-375/*RPN1* axis contributes to HCC progression (18). Disulfidptosis-associated genes containing *RPN1* have been used in risk models related to prognosis and immune characteristics of brain glioma (19) and HCC (20) patients, serving as independent prognostic factors for glioma. However, the comprehensive expression profile of *RPN1* across pan-cancers, its clinical relevance, and its relationship with the tumor microenvironment remain unclear. In this study, we further examined the differential expression and activity of *RPN1* across various cancer types. The results revealed strong mRNA expression of *RPN1* in 16 solid tumors, with significant differences between tumor tissues of specific cancer types and adjacent non-tumor tissues. Additionally, *RPN1* demonstrated robust activity in all analyzed tumor tissues. Validation from the GEO database confirmed consistent mRNA expression trends across 12 cancer types. *RPN1* exhibited significant diagnostic potential across 12 cancer types, particularly with high accuracy in GBM. Elevated *RPN1* expression in tumor tissues correlated with improved OS in DLBC and THYM, whereas it was associated with poorer prognosis in ACC, KICH, LGG, LIHC, and PAAD. Moreover, *RPN1* was linked to immune response, being enriched in immune-related pathways, correlating with immune scores in tumor tissues, and associated with various immune cells. Notably, in UCC, *RPN1* showed potential in predicting the efficacy of anti-PD-L1 immune therapy. In summary, these findings emphasized *RPN1*'s significance in pan-cancer scenarios and its implications for diagnosis, prognosis, and immune checkpoint inhibitor therapy. To our knowledge, this is the first study of *RPN1* in pan-cancers integrating data from

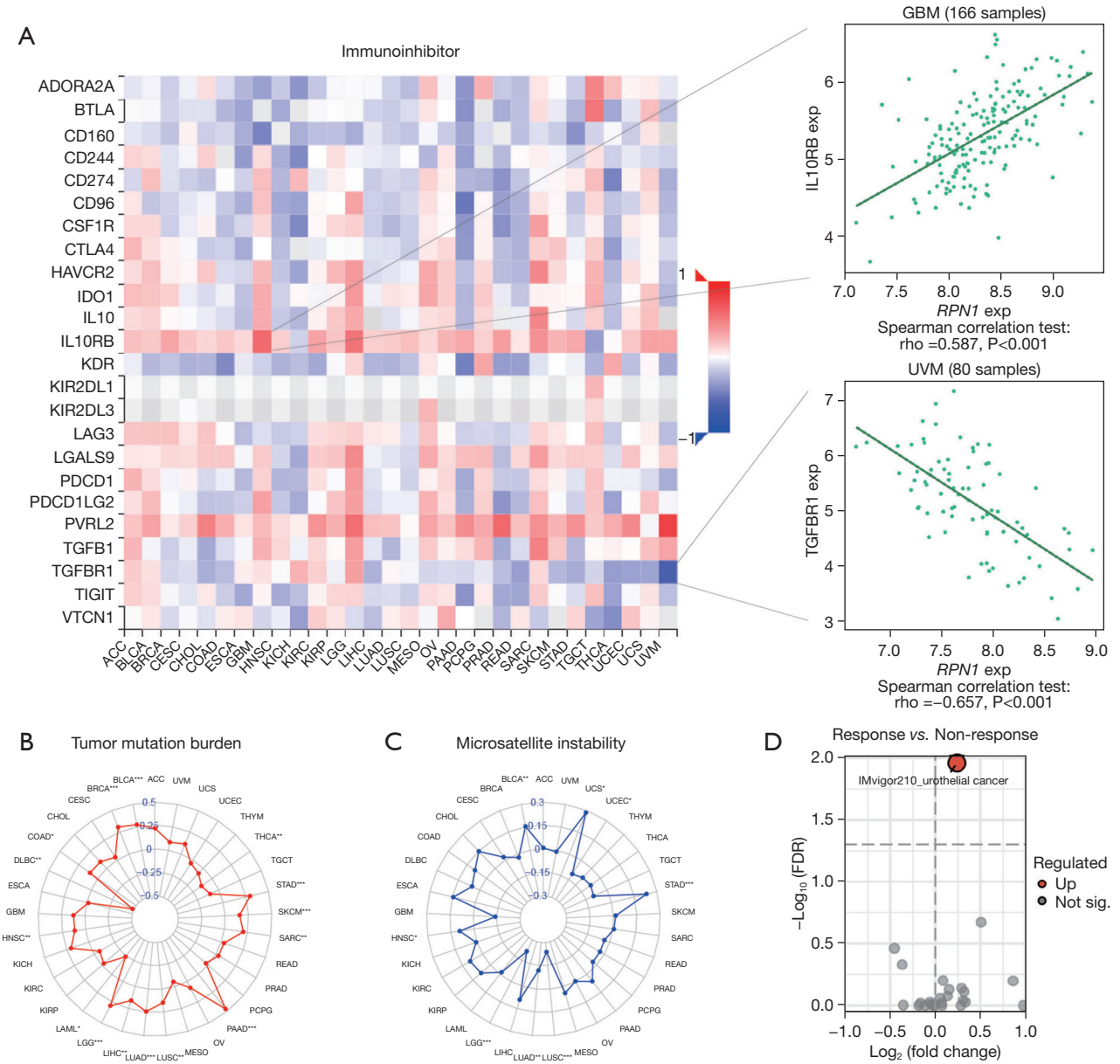

Figure 7 The potential immunotherapeutic implication of *RPN1*. (A) The correlations between the expressions of *RPN1* and immune inhibitors. Red indicates a positive correlation whereas blue indicates a negative correlation. The top 2 strongest associations are displayed via dot plots. Radar plots represented the relationships between *RPN1* expressions and tumor mutation burden (B) and microsatellite instability (C), respectively. The numbers are correlation coefficients, with negative values in the inner circle indicating negative correlation and positive values in the outer circle indicating positive correlation. Higher absolute values indicate a stronger correlation. (D) The scatter plot shows the levels of expression of *RPN1* in the responder and non-responder groups in 25 immunotherapy cohorts. An FDR-adjusted P value <0.05 is considered statistically significant. *, P<0.05; **, P<0.01; ***, P<0.001. exp, expression; FDR, false discovery rate; *RPN1*, ribophorin I.

multiple public gene databases.

Glucose deprivation is a common feature of the tumor microenvironment, which induces metabolic reprogramming in tumor cells to maintain redox balance (21). For instance, tumor cells acquire glutathione as a protective mechanism by upregulating *SLC7A11* expression (22), or adopt alternative strategies like *IDH1* and *ME1* to support NADPH formation (23). As suggested by the authors (3), future

investigations should explore whether other metabolic stress conditions that deplete intracellular NADPH levels can induce dual sulfur death. However, it is crucial to note that the heterogeneity in the protective mechanisms employed by different tumor cells to maintain redox balance, especially in the context of pan-cancer. Therefore, the universal significance of inducing dual sulfur death under glucose deprivation as a novel therapeutic target for cancer needs clarification. Considering the dependency of dual sulfur death on the *RPN1* gene, we examined the mRNA and protein expression levels of *RPN1* across various cancer types to identify tumor types with potential for inducing dual sulfur death therapy. Importantly, we demonstrated inhibition of dual sulfur death upon *RPN1* knockout in cell lines not validated in previous studies, regardless of *SLC7A11* expression levels. This provides additional evidence for *RPN1* as a potential universal target for cancer therapy. Furthermore, our study highlights the potential of *RPN1* as an immune therapy marker, although further validation in cohorts is required.

This study has several limitations. Firstly, we did not further validate the differential expression of *RPN1* in tumor and adjacent tissues obtained from our own tissue samples, which were used to verify the bioinformatics analysis. Specifically, investigating the expression of RPN1 in cohorts undergoing anti-PD-L1 therapy to validate its biomarker value in the real world was not performed. Secondly, some tumor types did not receive consistent validation across multiple databases, which may be related to systematic sampling biases. Finally, the detailed mechanism by which *RPN1* promotes disulfidptosis through inducing cell skeleton breakdown requires further elucidation.

Conclusions

Overall, these findings emphasize *RPN1*'s significance in disulfidptosis induction, its pan-cancer relevance, and implications for diagnosis, prognosis, and immune therapy.

Acknowledgments

Funding: None.

Footnote

Reporting Checklist: The authors have completed the MDAR reporting checklist. Available at https://tcr.amegroups.com/article/view/10.21037/tcr-24-581/rc

Data Sharing Statement: Available at https://tcr.amegroups.com/article/view/10.21037/tcr-24-581/dss

Peer Review File: Available at https://tcr.amegroups.com/article/view/10.21037/tcr-24-581/prf

Conflicts of Interest: All authors have completed the ICMJE uniform disclosure form (available at https://tcr.amegroups.com/article/view/10.21037/tcr-24-581/coif). The authors have no conflicts of interest to declare.

Ethical Statement: The authors are accountable for all aspects of the work in ensuring that questions related to the accuracy or integrity of any part of the work are appropriately investigated and resolved. The study was conducted in accordance with the Declaration of Helsinki (as revised in 2013).

References

1. Machesky LM. Deadly actin collapse by disulfidptosis. Nat Cell Biol 2023;25:375-6.
2. Zhang R, Kang R, Tang D. Reductive cell death: the other side of the coin. Cancer Gene Ther 2023;30:929-31.
3. Liu X, Nie L, Zhang Y, et al. Actin cytoskeleton vulnerability to disulfide stress mediates disulfidptosis. Nat Cell Biol 2023;25:404-14.
4. Qin Q, Li R, Li L, et al. Multi-target regulation of pro-inflammatory cytokine production by transcription factor Blimp-1. Inflamm Res 2023;72:217-20.
5. Orth-He EL, Huang HC, Rao SD, et al. Protein folding stress potentiates NLRP1 and CARD8 inflammasome activation. Cell Rep 2023;42:111965.
6. Liao KC, Mogridge J. Activation of the Nlrp1b inflammasome by reduction of cytosolic ATP. Infect Immun 2013;81:570-9.
7. Lillo S, Saleh M. Inflammasomes in Cancer Progression and Anti-Tumor Immunity. Front Cell Dev Biol

2022;10:839041.
8. Shen WJ, Zhang Y. RPN1 promotes the proliferation and invasion of breast cancer cells by activating the PI3K/AKT/mTOR signaling pathway. Discov Oncol 2024;15:25.
9. Zheng W, Zheng Y, Bai X, et al. RPNs Levels Are Prognostic and Diagnostic Markers for Hepatocellular Carcinoma. J Oncol 2022;2022:7270541.
10. Cancer Genome Atlas Research Network, Weinstein JN, Collisson EA, et al. The Cancer Genome Atlas Pan-Cancer analysis project. Nat Genet 2013;45:1113-20.
11. Clough E, Barrett T, Wilhite SE, et al. NCBI GEO: archive for gene expression and epigenomics data sets: 23-year update. Nucleic Acids Res 2024;52:D138-44.
12. Hänzelmann S, Castelo R, Guinney J. GSVA: gene set variation analysis for microarray and RNA-seq data. BMC Bioinformatics 2013;14:7.
13. Yoshihara K, Shahmoradgoli M, Martínez E, et al. Inferring tumour purity and stromal and immune cell admixture from expression data. Nat Commun 2013;4:2612.
14. Newman AM, Liu CL, Green MR, et al. Robust enumeration of cell subsets from tissue expression profiles. Nat Methods 2015;12:453-7.
15. Bonneville R, Krook MA, Kautto EA, et al. Landscape of Microsatellite Instability Across 39 Cancer Types. JCO Precis Oncol 2017;2017:PO.17.00073.
16. Ramírez AS, Kowal J, Locher KP. Cryo-electron microscopy structures of human oligosaccharyltransferase complexes OST-A and OST-B. Science 2019;366:1372-5.
17. Ding J, Xu J, Deng Q, et al. Knockdown of Oligosaccharyltransferase Subunit Ribophorin 1 Induces Endoplasmic-Reticulum-Stress-Dependent Cell Apoptosis in Breast Cancer. Front Oncol 2021;11:722624.
18. Zheng C, Liang J, Yu S, et al. Circ-SNX27 sponging miR-375/RPN1 axis contributes to hepatocellular carcinoma progression. Korean J Physiol Pharmacol 2023;27:333-44.
19. Wang X, Yang J, Yang F, et al. The disulfidptosis-related signature predicts prognosis and immune features in glioma patients. Sci Rep 2023;13:17988.
20. Wang Y, Yuan Z, Zhu Q, et al. Disulfidptosis-related genes of prognostic signature and immune infiltration features in hepatocellular carcinoma supported by bulk and single-cell RNA sequencing data. J Gastrointest Oncol 2024;15:377-96.
21. Reinfeld BI, Madden MZ, Wolf MM, et al. Cell-programmed nutrient partitioning in the tumour microenvironment. Nature 2021;593:282-8.
22. Lang X, Green MD, Wang W, et al. Radiotherapy and Immunotherapy Promote Tumoral Lipid Oxidation and Ferroptosis via Synergistic Repression of SLC7A11. Cancer Discov 2019;9:1673-85.
23. Ying M, You D, Zhu X, et al. Lactate and glutamine support NADPH generation in cancer cells under glucose deprived conditions. Redox Biol 2021;46:102065.

Cite this article as: Wang X, Zhu HQ, Lin SM, Xia BY, Xu B. *RPN1*: a pan-cancer biomarker and disulfidptosis regulator. Transl Cancer Res 2024;13(5):2518-2534. doi: 10.21037/tcr-24-581

